

# High-Resolution Spectroscopy of Winds Associated with T Tauri Stars

Naoto Iguchi<sup>1</sup> and Yoichi Itoh<sup>2</sup>

<sup>1</sup> Graduate School of Science, Kobe University, 1-1 Rokkodai-cho, Nada-ku, Kobe, Hyogo 657-8501, Japan

<sup>2</sup> Nishi-Harima Astronomical Observatory, Center for Astronomy, University of Hyogo, 407-2, Nishigaichi, Sayo, Hyogo 679-5313, Japan; *yitoh@nhao.jp*

Received 2015 June 28; accepted 2015 September 4

**Abstract** We carried out optical high-resolution spectroscopy of T Tauri stars using the Subaru Telescope. Using archived data from the Keck Telescope and the Very Large Telescope, we detected forbidden lines of [S II] at 4069 Å, in addition to those of [O I] at 5577 Å and 6300 Å, for 13 T Tauri stars. We consider that low-velocity components of these forbidden lines emanate from the wind associated with T Tauri stars. Using two flux ratios of the three lines, we simultaneously determined the hydrogen density and temperature of the winds. The winds of T Tauri stars have a hydrogen density of  $2.5 \times 10^6 \text{ cm}^{-3} - 2.5 \times 10^9 \text{ cm}^{-3}$  and a temperature of 10 800–18 000 K. The mass loss rates by the wind are estimated to lie in the range from  $2.0 \times 10^{-10} M_{\odot} \text{ yr}^{-1}$  to  $1.4 \times 10^{-9} M_{\odot} \text{ yr}^{-1}$ . The mass loss rates are found to increase with increasing mass accretion rates. The ratio of the mass loss rate to the mass accretion rate is 0.001–0.1 for classical T Tauri stars and 0.1–1 for transitional disk objects.

**Key words:** stars: pre-main sequence — stars: emission lines

## 1 INTRODUCTION

An outflow is an energetic phenomenon associated with a T Tauri star (TTS). It removes angular momentum from the system, accelerating the stellar evolution. The outflows observed in the optical and infrared wavelengths are classified into the following two groups (Hartigan et al. 1995). The first is a jet, which is a high-velocity component of the outflow. It is well collimated and often extends hundreds of astronomical units (AUs). The jet emits forbidden lines in the optical and near-infrared wavelengths, such as the [O I] line at 6300 Å, the [S II] line at 6716 Å, the [S II] line at 6731 Å and the [N II] line at 6586 Å. The emission line of the jet is blue-shifted about  $200 \text{ km s}^{-1}$  relative to that of the central star and has a velocity width of  $\sim 150 \text{ km s}^{-1}$ . The second component of the outflow is called wind. It is considered that the wind emanates from an inner portion of a circumstellar disk, though its launching point has not yet been spatially resolved. It is not well-collimated and the motion of the gas is slow. Thus, the wind exhibits a low-velocity component of the lines. It also emits forbidden lines, such as the [O I] line at 6300 Å and the [O I] line at 5577 Å. In the millimeter wavelengths, molecular outflows are also detected toward many TTSs.

The hydrogen density and temperature of the gas are fundamental parameters of the outflow. Bacciotti & Eisloffel (1999) calculated the electron density, temperature and ionization fraction of a jet, using the fluxes of the [S II]6716, [S II]6731, [N II]6583 and [O I]6300 lines. Because both [S II]6716 and [S II]6731 lines are emitted

from the same excitation level, the flux ratio of these lines only depends on the electron density of the jet. After deriving the electron density, they calculated the temperature and ionization fraction of the jet using the flux ratios of the [N II] 6583, [O I]6300 and [S II]6731 lines. The estimated hydrogen densities and temperatures range between  $10^3$  and a few  $10^4 \text{ cm}^{-3}$  and between 9000 and 12 000 K, respectively.

Hartigan et al. (1995) estimated the mass loss rates of the jets from the luminosities of the [O I]6300 emission lines. They assumed an electron density of the jets of  $7 \times 10^4 \text{ cm}^{-3}$  for all TTSs, and calculated the masses of the jets. By multiplying the velocity by the mass and dividing by the length of the jet, they concluded that the mass loss rates are between  $10^{-8} M_{\odot} \text{ yr}^{-1}$  and  $10^{-10} M_{\odot} \text{ yr}^{-1}$ . Based on spectrophotometry in the blue region, Gullbring et al. (1998) estimated the mass accretion rates of 29 classical TTSs to typically be between  $10^{-9}$  and  $10^{-7} M_{\odot} \text{ yr}^{-1}$ . With these values, Cabrit (2002) claimed that the ratios of the mass loss rates to the mass accretion rates range from 0.01 to 1 for TTSs.

Kwan & Tademaru (1995) constructed a model of TTS wind, in which the mass loss rate is expressed as a function of the electron density and temperature of the wind. The forbidden lines with a critical density higher than  $10^6 \text{ cm}^{-3}$  are considered to be emitted in the wind region. The critical density of the [O I] line at 5577 Å is  $1.3 \times 10^8 \text{ cm}^{-3}$  and that of the [O I] line at 6300 Å is  $1.4 \times 10^6 \text{ cm}^{-3}$ , thus these lines are considered to have a wind origin.

However, the electron density and temperature of the wind have not been simultaneously determined from observations. The ratios of the flux of [O I]5577 to that of [O I]6300 for the low-velocity components are between 0.1 and 1 (Hartigan et al. 1995). The ratio of 0.1 corresponds to a temperature of 5000 K if the electron density is  $10^8 \text{ cm}^{-3}$ , or a temperature of 15 000 K if the electron density is  $10^6 \text{ cm}^{-3}$ . With only two emission lines, one cannot determine the density and temperature of the wind simultaneously.

In addition to the [O I] lines at 5577 Å and 6300 Å, we investigate the [S II] line at 4069 Å. Its critical density is  $6.9 \times 10^6 \text{ cm}^{-3}$ . We assume that the low velocity components of the [S II] line at 4069 Å and the [O I] lines at 5577 Å and 6300 Å are signatures of a disk wind. By using three emission lines, the density and temperature can be determined simultaneously.

The observations and archived data are described in Section 2. We present the results in Section 3. In Section 4, we discuss the hydrogen density, the temperature, and the mass loss rates of the winds.

## 2 OBSERVATIONS AND ARCHIVED DATA

We carried out optical high-resolution spectroscopy of seven TTSs using the High Dispersion Spectrograph (HDS) mounted on the Subaru Telescope. The targets are single TTSs with spectral types of late K or early M. The data were obtained on 2012 September 8, with the StdTd mode and a slit width of  $0.6''$ . This setting of the instrument achieved the wavelength coverage of 4020–6780 Å with a spectral resolution of  $\sim 60\,000$ . The integration time for each object was between 600 s and 1600 s.

We also used archived data for nine TTSs obtained using the High Resolution Echelle Spectrometer (HIRES) mounted on the Keck Telescope. The spectral types of the targets are between K5 and M3.5. The data were acquired by G. J. Herczeg on 2008 January 23, G. W. Marcy on 2008 May 23 and 2008 December 3, S. E. Dahm on 2010 February 4, and T. E. Armandroff on 2010 December 2. The spectral ranges covered the [S II] line at 4069 Å, the [O I] line at 5577 Å, and the [O I] line at 6300 Å. The spectral resolution was  $\sim 70\,000$ . The integration time for each object was between 300 s and 1800 s. In addition, we used archived data of field dwarfs with spectral types identical to those of the TTSs.

Archive data for two TTSs obtained with the Ultraviolet and Visual Echelle Spectrograph (UVES) mounted on the Very Large Telescope (VLT) were also used. The data were acquired by N. E. Piskunov on 2000 April 16 and H. C. Stempels on 2002 April 19. The spectral resolution was  $\sim 80\,000$ . The integration times were 1800 s and 1900 s. Dwarf spectra acquired by C. Melo on 2009 April 2 were also used. The observed TTSs are summarized in Table 1. Among them, five objects are classified as transitional disk objects.

We reduced the HDS data in a standard manner; i.e., overscan subtraction, bias subtraction, flat fielding, re-

moval of scattered light, extraction of spectra, wavelength calibration using lines of the Th-Ar lamp, and continuum normalization. We used IRAF packages for all procedures. A detailed description of the data reduction method can be found in Takagi et al. (2011). The HIRES data were reduced using the Mauna Kea Echelle Extraction (MAKEE) package. The UVES data were reduced using the Gasgano package.

The emission lines of the [O I] line at 6300 Å are superimposed on telluric H<sub>2</sub>O lines. We removed the telluric lines by dividing the object spectra by the spectrum of S Mon, which is a fast-rotating O-type star.

A spectrum of a TTS consists of stellar continuum, photospheric absorption lines, forbidden emission lines, and continuum excesses due to the boundary layer and the circumstellar disk. To extract the forbidden emission lines from the spectra, we removed the continuum excess and filled the photospheric absorption lines using the spectrum of a field dwarf with the same spectral type. The continuum excess veils the intrinsic photospheric absorption lines. Flux of the stellar continuum and the strengths of the absorption lines, and thus also strengths of the forbidden emission lines, cannot be estimated unless the amount of the continuum excess is determined precisely. The estimation procedure of the amount of continuum excess consists of several steps. First, we estimated the radial velocities of the TTSs and the field dwarfs from the wavelengths of several absorption lines around 4069 Å, 5577 Å and 6300 Å. The spectra of the TTSs and the field dwarfs were shifted, so that their radial velocities were zero. The widths of the absorption lines were then measured. It is known that TTSs are often fast rotators. The field dwarf spectra were convolved with a Gaussian profile so that the full-width at half-maximum of the photospheric absorption lines were comparable with those of the TTS spectra. We were then able to create a veiled spectrum of a dwarf,  $S'$ , using the convolved field dwarf spectrum,  $S$ , as follows

$$S' = \frac{S + r}{1 + r}, \quad (1)$$

where  $r$  is the amount of veiling. We calculated  $r$  by comparing the equivalent widths of absorption lines near the forbidden lines in the TTS spectrum with those in the field dwarf spectrum. The veiled dwarf spectrum was subtracted from the TTS spectrum, then we added unity. With this process, photospheric features remained for five TTSs. For the other TTSs, the photospheric absorption lines were removed, as well as continuum excess.

We measured the equivalent widths of the forbidden lines by fitting the line profiles using Gaussian functions.

## 3 RESULTS

Figure 1 shows the forbidden line spectra of the classical TTSs and the transitional disk objects, where the photospheric absorption lines were subtracted. Some forbidden lines exhibited a low-velocity (narrow) component in addition to a high-velocity (broad) component. We consider

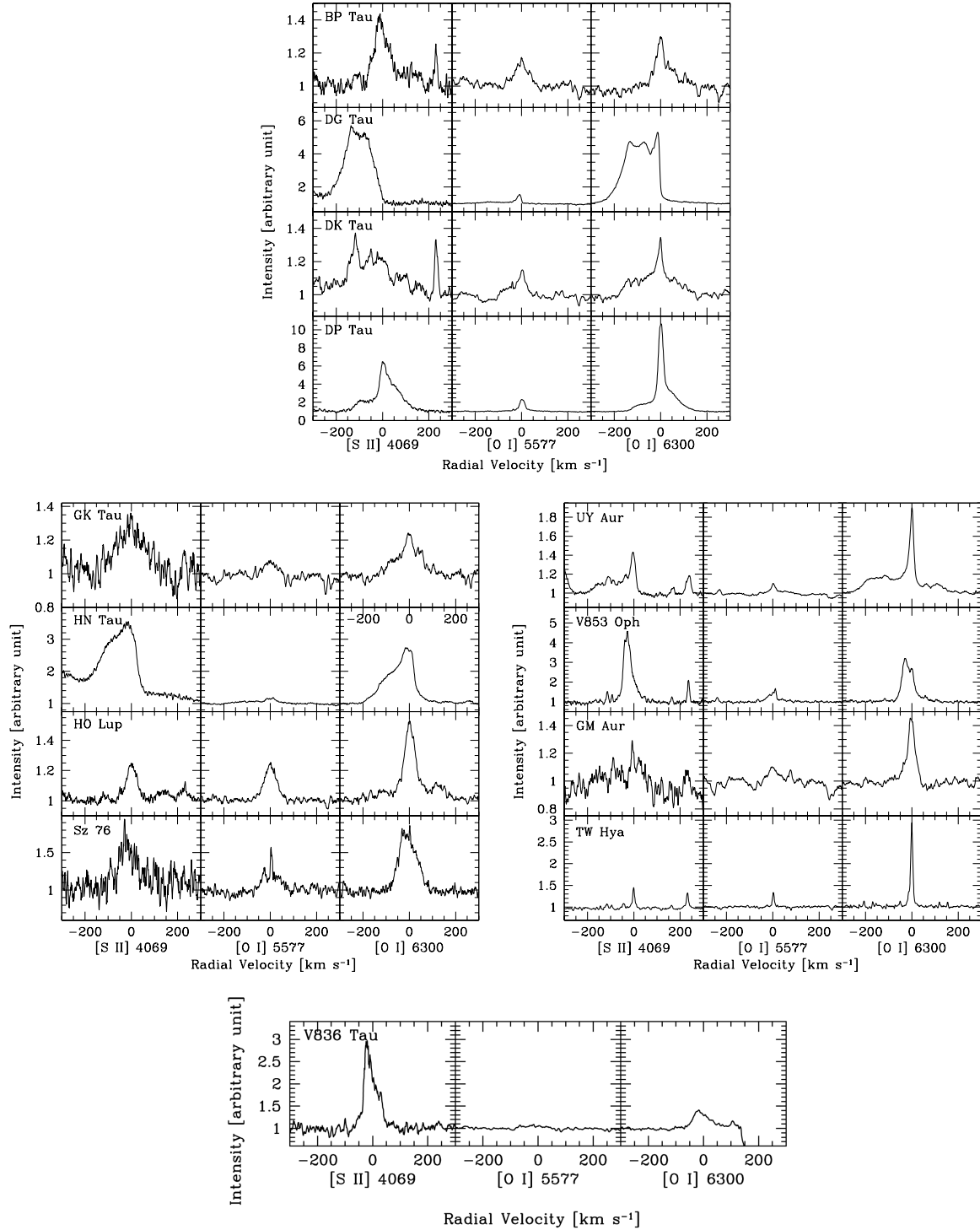


**Fig. 1** Forbidden emission lines of TTSs. Photospheric absorption lines and the continuum excess were subtracted and the continuum levels were normalized to unity.

that the low-velocity component has a wind origin and the high-velocity component has a jet origin. Equivalent widths of the forbidden lines are listed in Table 2. The amount of veiling is tabulated in Table 3.

The fluxes of the forbidden lines were calculated. We first corrected the interstellar extinction for each object. The amounts of extinction at the  $V$ -band ( $A_V$ ) were referred from Geoffroy & Monin (2001), Kenyon & Hartmann (1995), Hughes et al. (1994), Hamann &

**Table 1** Targets

| Object                    | Spectral Type | $V$ -mag | $A_V$ | $\log \dot{M}_{\text{acc}} [M_{\odot} \text{ yr}^{-1}]$ | Telescope/Instrument |
|---------------------------|---------------|----------|-------|---|----------------------|
| Classical T Tauri Stars   |               |          |       |   |                      |
| BP Tau                    | K7            | 12.16    | 0.49  | -7.54   | Keck/HIRES           |
| CI Tau                    | K7            | 12.99    | 2.10  | —   | Subaru/HDS           |
| DE Tau                    | M1            | 13.04    | 0.59  | -7.59   | Subaru/HDS           |
| DG Tau                    | K5            | 12.43    | 1.60  | -6.30   | Subaru/HDS           |
| DK Tau                    | K6            | 12.35    | 0.76  | -7.42   | Keck/HIRES           |
| DP Tau                    | M0            | 14.22    | 1.46  | -7.88   | Keck/HIRES           |
| DR Tau                    | K7            | 11.61    | 1.00  | -6.50   | Subaru/HDS           |
| GK Tau                    | K7            | 12.54    | 0.87  | -8.19   | Keck/HIRES           |
| HN Tau                    | K5            | 13.85    | 0.52  | -8.89   | Keck/HIRES           |
| HO Lup                    | K7            | 13.00    | 1.60  | -6.74   | VLT/UVES             |
| Sz 76                     | M1            | 15.18    | 1.90  | —   | Keck/HIRES           |
| UY Aur                    | K7            | 12.99    | 1.35  | -7.18   | Subaru/HDS           |
| V853 Oph                  | M3.75         | 13.65    | 2.00  | —   | Keck/HIRES           |
| Transitional Disk Objects |               |          |       |   |                      |
| DN Tau                    | K7            | 11.41    | 0.49  | —   | Subaru/HDS           |
| GM Aur                    | K7            | 12.03    | 0.14  | -8.02   | Subaru/HDS           |
| LkCa 15                   | K5            | 12.41    | 0.62  | —   | Keck/HIRES           |
| TW Hya                    | K7            | 11.27    | 0.00  | -8.82   | VLT/UVES             |
| V836 Tau                  | K7            | 13.12    | 0.59  | -9.80   | Keck/HIRES           |

Persson (1992) and Kitamura et al. (1996). Extinctions at the  $B$ - and  $R$ -bands were then calculated from that at the  $V$ -band with the extinction law of Rieke & Lebofsky (1985). Extinctions at the  $B$ -,  $V$ - and  $R$ -bands were applied to the  $B$ -,  $V$ - and  $R$ -band magnitudes of the objects. These bands correspond to the forbidden lines of [S II] at 4069 Å, [O I] at 5577 Å and [O I] at 6300 Å, respectively. Assuming that continuum emission was dominant in each band, we calculated the fluxes of the continuum level in the object spectra prior to the subtraction of the veiled dwarf spectrum. The fluxes of the forbidden lines were then estimated. The derived flux ratios of the low-velocity components for the forbidden lines after extinction correction are listed in Table 4.

#### 4 DISCUSSION

Veiling effect in wavelengths shorter than the  $I$ -band is attributed to the phenomenon of mass accretion (Bertout et al. 1988). The continuum excess due to mass accretion exhibits the spectral energy distribution of a blackbody with a temperature of 8000–10 000 K (Hartigan et al. 1991). Basri & Batalha (1990) measured the amount of the veiling of TTSs in optical wavelengths. They found that the ratio of the veiling to the photospheric continuum increases at wavelengths shorter than 5000 Å for several TTSs. It is considered that the major source of optical veiling is the boundary layer between the central star and the circumstellar disk. They also suggested that optical veiling is dependent on the accretion rate. We investigated the correlation between the mass accretion rate of the TTSs and the amount of veiling. The mass accretion rates were referred from Gullbring et al. (1998), Gullbring et al. (2000), Johns-Krull et al. (2000) and Herczeg & Hillenbrand (2008). In our sample, the dependence described above is not clearly seen. Instead, there is a correlation between the color of

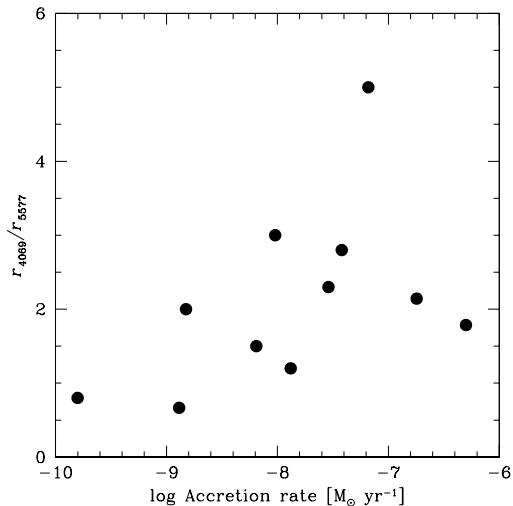


**Fig. 2** The ratio of the amount of veiling at 4069 Å to that at 5577 Å as a function of the mass accretion rate. The ratios increase as the temperature of the boundary layer increases.

the veiling and the mass accretion rates (Fig. 2). It is revealed that TTSs with high mass accretion rates exhibit a high-temperature continuum excess.

We simultaneously determined the hydrogen density and temperature of the wind using the two flux ratios of the low-velocity components of the three forbidden lines. We used the software package CLOUDY (Ferland et al. 1998) to calculate the emissivity of the forbidden lines, given the hydrogen density and temperature of the gas. We assumed that the three forbidden lines emanate from the same region. Thus, the ratios of the emissivities of the lines correspond to the flux ratios of the lines. We also assumed solar abundance of S and O. The ionization parameter of the program indicates the ratio of incident ionization pho-

**Table 2** Equivalent Widths of Low-velocity Components of the Forbidden Lines

| Object   | Equivalent width [Å]                   |  |  |
|----------|--|--|--|
|          | [S II] 4069 Å                          | [O I] 5577 Å                           | [O I] 6300 Å                           |
| BP Tau   | 0.42±0.04                              | 0.20±0.03                              | 0.37 <sup>+0.04</sup> <sub>-0.03</sub> |
| DG Tau   | 1.33 <sup>+0.23</sup> <sub>-0.11</sub> | 0.27±0.01                              | 1.70 <sup>+0.07</sup> <sub>-0.15</sub> |
| DK Tau   | 0.43 <sup>+0.04</sup> <sub>-0.05</sub> | 0.07±0.01                              | 0.44±0.03                              |
| DP Tau   | 3.80 <sup>+0.04</sup> <sub>-0.05</sub> | 0.77 <sup>+0.03</sup> <sub>-0.04</sub> | 3.90±0.10                              |
| GK Tau   | 0.58 <sup>+0.17</sup> <sub>-0.14</sub> | 0.08 <sup>+0.03</sup> <sub>-0.02</sub> | 0.48 <sup>+0.05</sup> <sub>-0.06</sub> |
| HN Tau   | 1.30 <sup>+0.06</sup> <sub>-0.02</sub> | 0.21 <sup>+0.04</sup> <sub>-0.08</sub> | 1.24 <sup>+0.07</sup> <sub>-0.05</sub> |
| HO Lup   | 0.19±0.02                              | 0.29±0.02                              | 0.63 <sup>+0.03</sup> <sub>-0.02</sub> |
| Sz 76    | 0.75 <sup>+0.24</sup> <sub>-0.16</sub> | 0.42±0.04                              | 1.49 <sup>+0.09</sup> <sub>-0.04</sub> |
| UY Aur   | 0.16 <sup>+0.01</sup> <sub>-0.03</sub> | 0.05±0.01                              | 0.33 <sup>+0.04</sup> <sub>-0.03</sub> |
| V853 Oph | 2.00 <sup>+0.06</sup> <sub>-0.03</sub> | 0.44±0.05                              | 2.60 <sup>+0.05</sup> <sub>-0.06</sub> |
| GM Aur   | 0.07±0.02                              | 0.09 <sup>+0.03</sup> <sub>-0.02</sub> | 0.38±0.02                              |
| TW Hya   | 0.07±0.01                              | 0.07±0.01                              | 0.47 <sup>+0.02</sup> <sub>-0.01</sub> |
| V836 Tau | 1.25 <sup>+0.08</sup> <sub>-0.05</sub> | 0.12±0.04                              | 0.59 <sup>+0.05</sup> <sub>-0.03</sub> |

**Table 3** Amount of Continuum Veiling Near the Forbidden Lines

| Object   | [S II] 4069 Å | [O I] 5577 Å | [O I] 6300 Å |
|----------|---------------|--------------|--------------|
| BP Tau   | 2.3           | 1.0          | 0.5          |
| DG Tau   | 5.0           | 2.8          | 2.5          |
| DK Tau   | 1.4           | 0.5          | 0.3          |
| DP Tau   | 3.0           | 2.5          | 1.0          |
| GK Tau   | 1.5           | 1.0          | 0.5          |
| HN Tau   | 2.0           | 3.0          | 1.2          |
| HO Lup   | 7.5           | 3.5          | 1.6          |
| Sz 76    | 0.1           | 0.4          | 0.2          |
| UY Aur   | 9.0           | 1.8          | 1.1          |
| V853 Oph | 2.0           | 1.5          | 0.9          |
| GM Aur   | 0.9           | 0.3          | 0.3          |
| TW Hya   | 0.8           | 0.4          | 0.25         |
| V836 Tau | 0.2           | 0.25         | 0            |

**Table 4** Flux Ratios of the Forbidden Lines

| Object   | [S II] 4069 / [O I] 6300               | [O I] 5577 / [O I] 6300                |
|----------|--|--|
| BP Tau   | 0.73 <sup>+0.07</sup> <sub>-0.09</sub> | 0.46 <sup>+0.07</sup> <sub>-0.06</sub> |
| DG Tau   | 0.88 <sup>+0.14</sup> <sub>-0.06</sub> | 0.17±0.01                              |
| DK Tau   | 0.59 <sup>+0.05</sup> <sub>-0.06</sub> | 0.15 <sup>+0.02</sup> <sub>-0.01</sub> |
| DP Tau   | 0.63 <sup>+0.05</sup> <sub>-0.03</sub> | 0.17±0.01                              |
| GK Tau   | 0.60 <sup>+0.15</sup> <sub>-0.12</sub> | 0.14 <sup>+0.04</sup> <sub>-0.03</sub> |
| HN Tau   | 0.72 <sup>+0.05</sup> <sub>-0.01</sub> | 0.14 <sup>+0.02</sup> <sub>-0.04</sub> |
| HO Lup   | 0.40 <sup>+0.08</sup> <sub>-0.03</sub> | 0.40 <sup>+0.06</sup> <sub>-0.04</sub> |
| Sz 76    | 0.34 <sup>+0.07</sup> <sub>-0.05</sub> | 0.20 <sup>+0.01</sup> <sub>-0.02</sub> |
| UY Aur   | 0.33 <sup>+0.01</sup> <sub>-0.05</sub> | 0.13±0.02                              |
| V853 Oph | 2.88 <sup>+0.09</sup> <sub>-0.06</sub> | 0.33 <sup>+0.03</sup> <sub>-0.02</sub> |
| GM Aur   | 0.08 <sup>+0.03</sup> <sub>-0.01</sub> | 0.20 <sup>+0.05</sup> <sub>-0.03</sub> |
| TW Hya   | 0.09 <sup>+0.00</sup> <sub>-0.01</sub> | 0.09±0.01                              |
| V836 Tau | 0.88±0.06                              | 0.17 <sup>+0.03</sup> <sub>-0.04</sub> |

ton density to the hydrogen density of a gas. We set it to  $10^{-15}$ . The emissivities of the [S II]4069, [O I]5577 and [O I]6300 lines were calculated for the hydrogen density between  $10^3 \text{ cm}^{-3}$  and  $10^{11} \text{ cm}^{-3}$  with 0.2 dex intervals and for the temperature between 6000 K and 20 000 K with an interval of 500 K.

**Table 5** Estimated Hydrogen Density and Temperature of the Winds

| Object   | $\log(N_{\text{H}}) [\text{cm}^{-3}]$  | $T$ [K]                                |
|----------|--|--|
| BP Tau   | 7.78 <sup>+0.22</sup> <sub>-0.38</sub> | 13000 <sup>+1000</sup> <sub>-500</sub> |
| DG Tau   | 6.4 <sup>+0.3</sup> <sub>-0.1</sub>    | 15000 <sup>+1000</sup> <sub>-0</sub>   |
| DK Tau   | 7.78 <sup>+0.62</sup> <sub>-1.30</sub> | 12200 <sup>+2300</sup> <sub>-700</sub> |
| DP Tau   | 7.0 <sup>+0.3</sup> <sub>-0.4</sub>    | 14000±500                              |
| GK Tau   | 7.78 <sup>+1.1</sup> <sub>-1.48</sub>  | 12500 <sup>+2750</sup> <sub>-250</sub> |
| HN Tau   | 6.48 <sup>+0.22</sup> <sub>-0.48</sub> | 15000±500                              |
| HO Lup   | 8.7 <sup>+0.18</sup> <sub>-0.3</sub>   | 11500 <sup>+500</sup> <sub>-0</sub>    |
| Sz 76    | 8.48 <sup>+0.12</sup> <sub>-0.48</sub> | 11500 <sup>+500</sup> <sub>-250</sub>  |
| UY Aur   | 8.0 <sup>+0.48</sup> <sub>-0.15</sub>  | 11800 <sup>+200</sup> <sub>-300</sub>  |
| V853 Oph | 6.48 <sup>+0.06</sup> <sub>-0.08</sub> | 18000±250                              |
| GM Aur   | 9.4 <sup>+0.2</sup> <sub>-0.4</sub>    | 10800 <sup>+200</sup> <sub>-300</sub>  |
| TW Hya   | 8.78 <sup>+0.22</sup> <sub>-0.08</sub> | 11000±250                              |
| V836 Tau | 6.48 <sup>+0.22</sup> <sub>-0.48</sub> | 15250±750                              |

As an example, the case of BP Tau is shown in Figure 3. The ratio of the observed flux of the [O I]5577 line to that of the [O I]6300 line is 0.46, and the ratio of the observed flux of the [S II]4069 line to that of the [O I]6300 line is 0.73, after extinction correction. Such ratios are reproduced when the hydrogen density of the gas is  $(6.0_{-3.5}^{+4.0}) \times 10^7 \text{ cm}^{-3}$  and the temperature is  $13000_{-500}^{+1000} \text{ K}$ . We find that neither the hydrogen density nor the temperature change with the ionization parameter, unless it exceeds  $10^{-11}$ . With an ionization parameter larger than  $10^{-9}$ , no combination of parameters of the hydrogen density and temperature of the gas can reproduce the two observed ratios of line fluxes. In the same manner, we determine the hydrogen density and temperature of the wind for the 13 TTSS (Table 5). The hydrogen densities of the winds are found to be between  $2.5 \times 10^6$  and  $2.5 \times 10^9 \text{ cm}^{-3}$ . The wind temperatures are found to be between 10 800 K and 18 000 K. For the transitional disk objects, the density and temperature of the wind are calculated for the three objects. The resulting temperatures of two transitional disk objects appear low among the targets. However, there is neither a correlation between the mass accretion rate and the hydrogen density of the wind nor mass accretion rate and the wind temperature, for the whole sample.

Krasnopolsky et al. (2003) simulated an axisymmetric outflow which was magnetocentrally driven from an inner portion of an accretion disk around a TTS. The hydrogen density of the outflow was calculated to be  $10^6 \text{ cm}^{-3}$  at 5 AU from the central star and  $10^9 \text{ cm}^{-3}$  at the innermost region. These densities are consistent with the densities of the wind calculated from the observations described here. The isodensity region of the outflow is spherical, at least for the region with a density higher than  $10^6 \text{ cm}^{-3}$ .

Ferro-Fontán & Gómez de Castro (2003) investigated the thermal structure of the wind. The disk wind was found to have a temperature of  $\sim 10000 \text{ K}$  in the densest region ( $10^9 \text{ cm}^{-3}$ ) and  $\sim 15000 \text{ K}$  in the less dense region ( $10^6 \text{ cm}^{-3}$ ). These temperatures are consistent with the ob-

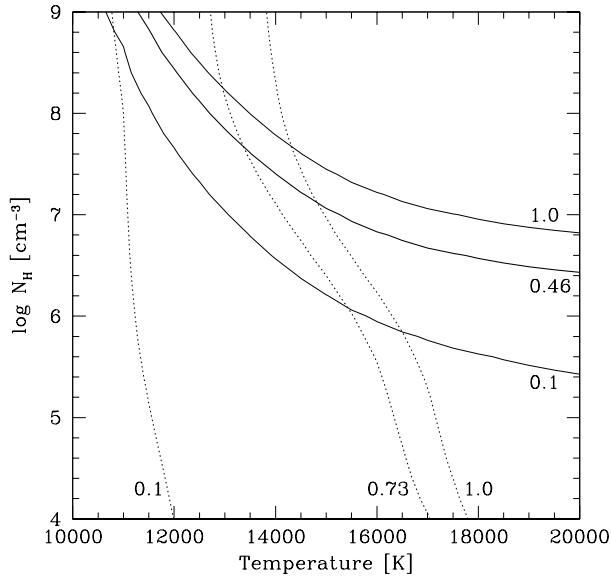


**Fig. 3** The flux ratios of three forbidden lines emanating from BP Tau. The thick solid line indicates  $[\text{O I}] 5577 / [\text{O I}] 6300 = 0.46$ . The thin lines show the ratios of 0.1 and 1.0. The thick dotted line indicates  $[\text{S II}] 4069 / [\text{O I}] 6300 = 0.73$ , and the thin dotted lines show the ratios of 0.1 and 1.0. From this figure, the hydrogen density of the wind is found to be  $(6.0^{+4.0}_{-3.5}) \times 10^7 \text{ cm}^{-3}$  and the temperature is found to be  $13000^{+1000}_{-500} \text{ K}$ .

served temperatures of the wind. The consistency of the hydrogen density and temperature of the winds between the observations and the simulations supports the idea that the TTS wind emanates from the inner portion of the circumstellar disk. Note that the hydrogen density and temperature of the winds calculated from the observations correspond to the average values of the wind region; this is because the spatial resolution of the observations is as large as a hundred AU.

We estimated the mass and the mass loss rate of the wind. We used the flux of the  $[\text{O I}] 6300$  line for the mass estimates. The fluxes of the forbidden line were translated into the luminosity of the line, given the distance. We assumed that the distance to the Taurus molecular cloud is 140 pc (Elias 1978), that to the Lupus molecular cloud is 150 pc (Crawford 2000), that to V853 Oph is 135 pc (Mamajek 2008), and that to TW Hya is 54 pc (van Leeuwen 2007). By dividing the luminosity of the line by the emissivity of the line, one derives the volume of the emission region. The volumes range from  $3.3 \times 10^{37} \text{ cm}^3$  to  $6.4 \times 10^{41} \text{ cm}^3$ . Assuming a spherical emission region, the radius was estimated to be between 0.22 AU and 5.7 AU. Note that this extent is consistent with the radius of the region from which the wind with a density of  $10^6 \text{ cm}^{-3}$  and higher emanates (Krasnopolsky et al. 2003). By multiplying this volume by the hydrogen density, the masses were estimated to be between  $4.7 \times 10^{-11} M_\odot$  and  $1.3 \times 10^{-9} M_\odot$ . Assuming that the wind emanates from the surface of the circumstellar disk with a vertical speed of  $10 \text{ km s}^{-1}$ , the mass loss rates were derived to be be-

tween  $2.0 \times 10^{-10} M_\odot \text{ yr}^{-1}$  and  $1.4 \times 10^{-9} M_\odot \text{ yr}^{-1}$ . The emissivity and luminosity of the  $[\text{O I}] 6300$  line are listed in Table 6, as well as the masses and the mass loss rates of the wind.

Figure 4 shows the relationship between the mass accretion rates and the mass loss rates. The ratios of the mass loss rate to the mass accretion rate are 0.001 – 0.1 for the classical TTSs and 0.1 – 1 for the transitional disk objects. We claim that the wind is one of the dominant mass loss processes of the system, at least for transitional disk objects. The ratio of the wind mass loss rate to the accretion rate has also been investigated from theoretical approaches and numerical simulations. Pelletier & Pudritz (1992) constructed a model of a centrifugally driven hydromagnetic wind from a Keplerian accretion disk. They found that the ratio of the mass loss rate to the mass accretion rate is  $\sim 0.1$ . Sheikhezami et al. (2012) carried out numerical simulations of a jet and an outflow from an accretion disk. They found that 10% – 50% of the accreted material is diverted into the jet or the wind. These values are roughly consistent with the ratios of the mass loss rate to the mass accretion rate derived from the observations.

We also found from the observations that the mass loss rates gradually increase with increasing mass accretion rates, as described by

$$\dot{M}_{\text{loss}} [M_\odot \text{ yr}^{-1}] = 10^{-7.95} \times \dot{M}_{\text{accretion}}^{0.17} [M_\odot \text{ yr}^{-1}]. \quad (2)$$

Ferreira & Pelletier (1995) introduced the ejection index,  $\xi$ ,

$$\frac{\dot{M}_{\text{loss}}}{\dot{M}_{\text{accretion}}} = 1 - \left( \frac{r_i}{r_e} \right)^\xi, \quad (3)$$

where  $r_i$  is the innermost radius of the disk and  $r_e$  is the outermost radius. Assuming  $\frac{r_i}{r_e} = \frac{1}{30}$  as in the case of Sheikhezami et al. (2012), we find  $\xi = 0.12$  for  $\dot{M}_{\text{accretion}} = 10^{-9} M_\odot \text{ yr}^{-1}$ . Ferreira (1997) constrained the ejection index to  $0.004 < \xi < 0.08$  for a magnetically-driven jet. On the other hand, Sheikhezami et al. (2012) derived  $0.1 < \xi < 0.5$ . The value of  $\xi$  calculated from the observations is roughly consistent with these expected values. On the other hand, we find  $\xi = 3.5 \times 10^{-4}$  for  $\dot{M}_{\text{accretion}} = 10^{-6} M_\odot \text{ yr}^{-1}$ . Such a small value of  $\xi$  is not predicted by theoretical studies. However, we noticed that some objects with a small  $\xi$  have high-velocity components of the forbidden lines. Thus, it is considered that these objects have jets, which are the main contributor of the mass loss process. A calculation of the mass loss rates based on unambiguously determined densities and temperatures of the winds and jets for many TTSs is necessary to constrain the ejection index, the conditions of the inner disk, and the mechanism causing the phenomenon of outflow.

## 5 CONCLUSIONS

We measured the fluxes of three forbidden lines of 13 TTSs with high resolution optical spectroscopy. If the low velocity components of the lines are in fact signatures of a disk wind, the following conclusions apply.

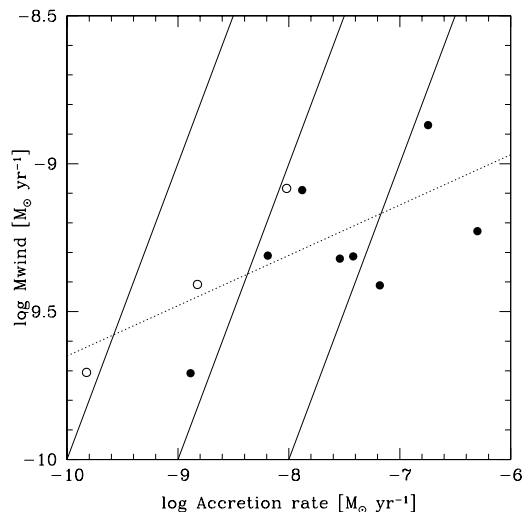


**Fig. 4** The mass loss rate of the wind as a function of the mass accretion rate from the circumstellar disk. The filled circles represent the classical TTSs and the open circles represent the transitional disk objects. The dotted line indicates the relationship between the mass loss rates and the mass accretion rates (Equation (2)).

**Table 6** Estimated Mass and Mass Loss Rate of the Winds

| Object   | $\log \epsilon_{[\text{OI}]6300}$<br>[ $\text{erg s}^{-1}$ ] | $\log L_{[\text{OI}]6300}$<br>[ $L_{\odot}$ ] | $\log \dot{M}_{\text{loss}}$<br>[ $M_{\odot} \text{ yr}^{-1}$ ] | $\log \dot{M}_{\text{acc}}$<br>[ $M_{\odot} \text{ yr}^{-1}$ ] |
|----------|--|---|---|--|
| BP Tau   | -10.7  | -4.69   | -9.3  | -7.54  |
| DG Tau   | -12  | -3.78   | -9.2  | -6.3   |
| DK Tau   | -10.55   | -4.53   | -9.3  | -7.42  |
| DP Tau   | -10.7  | -4.08   | -9.1  | -7.88  |
| GK Tau   | -10.55   | -4.53   | -9.3  | -8.19  |
| HN Tau   | -12.2  | -4.82   | -9.7  | -8.89  |
| HO Lup   | -9.6   | -4.29   | -8.9  | -6.74  |
| Sz 76    | -10.05   | -4.59   | -9.0  | —  |
| UY Aur   | -10.3  | -4.76   | -9.4  | -7.18  |
| V853 Oph | -12.4  | -4.22   | -9.2  | —  |
| GM Aur   | -8.7   | -4.76   | -9.1  | -8.02  |
| TW Hya   | -9.5   | -5.12   | -9.4  | -8.82  |
| V836 Tau | -12.2  | -4.81   | -9.7  | -9.8   |

- (1) The forbidden lines of [S II] at 4069 Å, [O I] at 5577 Å and [O I] at 6300 Å were detected. With two flux ratios of the three lines, the hydrogen density and temperature of the winds were determined simultaneously. The hydrogen densities of the winds were between  $2.5 \times 10^6 \text{ cm}^{-3}$  and  $2.5 \times 10^9 \text{ cm}^{-3}$ . The temperatures of the winds range from 10 800 K to 18 000 K.
- (2) Objects with high mass accretion rates exhibit high mass loss rates of the winds. The ratios of the mass loss rates of the winds to the mass accretion rates are between 0.001 and 0.1 for the classical TTSs, and between 0.1 and 1 for the transitional disk objects. These ratios are roughly consistent with the ratio derived from numerical simulations. The wind is one of the dominant processes of mass loss, at least for the transitional disk objects.
- (3) The objects with a high mass accretion rate exhibit high-temperature continuum excesses.

**Acknowledgements** We thank the staff members and operators at the Subaru Telescope. This research has made use of the Keck Observatory Archive (KOA), which is operated by the W. M. Keck Observatory and the NASA Exoplanet Science Institute (NExSci), under contract with the National Aeronautics and Space Administration.

## References

- Bacciotti, F., & Eisloffel, J. 1999, *A&A*, 342, 717  
 Basri, G., & Batalha, C. 1990, *ApJ*, 363, 654  
 Bertout, C., Basri, G., & Bouvier, J. 1988, *ApJ*, 330, 350  
 Cabrit, S. 2002, in *EAS Publications Series*, 3, EAS Publications Series, ed. J. Bouvier & J.-P. Zahn, 147  
 Crawford, I. A. 2000, *MNRAS*, 317, 996  
 Elias, J. H. 1978, *ApJ*, 224, 857  
 Ferland, G. J., Korista, K. T., Verner, D. A., et al. 1998, *PASP*, 110, 761

- Ferreira, J. 1997, *A&A*, 319, 340
- Ferreira, J., & Pelletier, G. 1995, *A&A*, 295, 807
- Ferro-Fontán, C., & Gómez de Castro, A. I. 2003, *MNRAS*, 342, 427
- Geoffray, H., & Monin, J.-L. 2001, *A&A*, 369, 239
- Gullbring, E., Hartmann, L., Briceño, C., & Calvet, N. 1998, *ApJ*, 492, 323
- Gullbring, E., Calvet, N., Muzerolle, J., & Hartmann, L. 2000, *ApJ*, 544, 927
- Hamann, F., & Persson, S. E. 1992, *ApJ*, 394, 628
- Hartigan, P., Edwards, S., & Ghandour, L. 1995, *ApJ*, 452, 736
- Hartigan, P., Kenyon, S. J., Hartmann, L., et al. 1991, *ApJ*, 382, 617
- Herczeg, G. J., & Hillenbrand, L. A. 2008, *ApJ*, 681, 594
- Hughes, J., Hartigan, P., Krautter, J., & Kelemen, J. 1994, *AJ*, 108, 1071
- Johns-Krull, C. M., Valenti, J. A., & Linsky, J. L. 2000, *ApJ*, 539, 815
- Kenyon, S. J., & Hartmann, L. 1995, *ApJS*, 101, 117
- Kitamura, Y., Kawabe, R., & Saito, M. 1996, *ApJ*, 465, L137
- Krasnopolsky, R., Li, Z.-Y., & Blandford, R. D. 2003, *ApJ*, 595, 631
- Kwan, J., & Tadamaru, E. 1995, *ApJ*, 454, 382
- Mamajek, E. E. 2008, *Astronomische Nachrichten*, 329, 10
- Pelletier, G., & Pudritz, R. E. 1992, *ApJ*, 394, 117
- Rieke, G. H., & Lebofsky, M. J. 1985, *ApJ*, 288, 618
- Sheikhnezami, S., Fendt, C., Porth, O., Vaidya, B., & Ghanbari, J. 2012, *ApJ*, 757, 65
- Takagi, Y., Itoh, Y., Oasa, Y., & Sugitani, K. 2011, *PASJ*, 63, 677
- van Leeuwen, F. 2007, *A&A*, 474, 653